



This is a repository copy of *A simple scalar coupled map lattice model for excitable media*.

White Rose Research Online URL for this paper:
<http://eprints.whiterose.ac.uk/74667/>

Monograph:

Guo, Y., Zhao, Y., Coca, D. et al. (1 more author) (2010) A simple scalar coupled map lattice model for excitable media. Research Report. ACSE Research Report no. 1016 . Automatic Control and Systems Engineering, University of Sheffield

Reuse

Unless indicated otherwise, fulltext items are protected by copyright with all rights reserved. The copyright exception in section 29 of the Copyright, Designs and Patents Act 1988 allows the making of a single copy solely for the purpose of non-commercial research or private study within the limits of fair dealing. The publisher or other rights-holder may allow further reproduction and re-use of this version - refer to the White Rose Research Online record for this item. Where records identify the publisher as the copyright holder, users can verify any specific terms of use on the publisher's website.

Takedown

If you consider content in White Rose Research Online to be in breach of UK law, please notify us by emailing eprints@whiterose.ac.uk including the URL of the record and the reason for the withdrawal request.



eprints@whiterose.ac.uk
<https://eprints.whiterose.ac.uk/>

A Simple Scalar Coupled Map Lattice Model for Excitable Media

Yuzhu Guo, Yifan Zhao, Daniel Coca, and S. A. Billings



Research Report No. 1016

Department of Automatic Control and Systems Engineering
The University of Sheffield
Mappin Street, Sheffield,
S1 3JD, UK

8 September 2010

A Simple Scalar Coupled Map Lattice Model for Excitable Media

Yuzhu Guo, Yifan Zhao, Daniel Coca, and S.A. Billings

*Department of Automatic Control and Systems Engineering,
University of Sheffield, Mapping Street,
Sheffield S1 3JD, UK*

Abstract

A simple scalar coupled map lattice model for excitable media is intensively analysed in this paper. This model is used to explain the excitability of excitable media, and a Hopf-like bifurcation is employed to study the different spatio-temporal patterns produced by the model. Several basic rules for the construction of these kinds of models are proposed. Illustrative examples demonstrate that the sCML model is capable of generating complex spatiotemporal patterns.

Keywords: Scalar coupled map lattice model; excitable media; pattern generation

1. Introduction

Excitable media are a very important class of nonlinear spatio-temporal dynamic systems which widely exist in biological, physical, chemical and ecological systems. A wide variety of patterns have been observed in excitable media including solitary patterns, target-like patterns, spiral waves, and so on. Many studies have shown that an enormous and complex range of macroscopic behaviours can be generated using relatively simple microscopic models.

Cells in excitable media can be characterised by three states: resting, excited and refractory. A cell in a resting state is stable for small perturbations while a perturbation with strength greater than a certain threshold can cause this cell to undergo a large excursion. Usually, the shape of the response does not depend on the perturbation strength, as long as the perturbation exceeds the

threshold. After this strong response, the system returns to its initial resting state. A subsequent excitation can be generated after a suitable length of time, called the refractory period, has passed. This property of excitable media is commonly called excitability. [Zykov, 2008]

Several kinds of models have been proposed to describe excitable media including partial differential equations (PDE), coupled map lattice (CML), cellular automata (CA), and cellular neural networks (CNN). The most commonly used models are reaction-diffusion equations where the local dynamics interact with the diffusive transportation to generate complex patterns. Excitable media are most naturally represented as partial differential equations, where the evolution of cells in the excitable media is modelled by coupled differential equations of a reaction-diffusion structure. Examples of partial differential equation models include the FHN model [FitzHugh, 1955] the Oregonator model [Field et al., 1972], the predator-prey models, the Barkley model [Barkley, 1991] and so on. The advantages of PDE models lie in the close connection with real systems. However PDE models for excitable media are always nonlinear and can be very complex. Furthermore the number of differential equations required to represent a cell in the system may be large. For example, the DiFrancesco-Noble model of Purkinje fibres has 14 dimensions and over a hundred parameters [DiFrancesco & Noble, 1985]. Therefore both simulation and identification of partial differential equation models is often a difficult task.

Discretising time and space coordinates of partial differential models yields the coupled map lattice model on a discrete time and space lattice. Owing to the computational efficiency and richness of dynamical behaviour, coupled map lattice models have been widely used for the description, simulation, and identification of excitable media [Kawasaki et al., 1990]. A CML model for excitable media usually needs more than one variable and some of these variables may not be measurable in practical systems. Consequently, some of the difficulties of PDE models in identification of real systems also exist in CML models.

Cellular automata defined on a discrete lattice can simplify the dynamic description of a system by mapping the system behaviour onto a few discrete states. In cellular automata models, the

continuous effects of diffusion are mapped to simple rules based on neighbourhood interactions. Typical cellular automata models include the Greenberg-Hasting model (GHM) [Greenberg & Hastings, 1978], Hodgepodge Machine Model (HMM), Cyclic Cellular Automata model, and the Gerhardt-Schuster-Tyson Model [Gerhardt et al., 1990]. On the one hand, cellular automata models are simple for the simulation of excitable media, on the other hand only a very limited number of parameters can be controlled when the neighbourhood is determined.

Cellular neural networks which share the best features of both neural networks and cellular automata are another important class of model for excitable media. A CNN is made up of a massive collection of regularly spaced circuit items which communicate with each other through nearest neighbours. CNNs are large-scale nonlinear analogue circuits which process signals in real time [Chua & Yang, 1988]. Simulation applications of CNNs have been developed into a wide range of disciplines [Fortuna et al., 2001]. CNNs also provide a link between nonlinear differential equations and discrete cellular automata [Chua, 2007]. However, procedures are required to efficiently learn suitable template values for complex CNN applications.

Excitable media have been widely and intensively studied including theoretical analysis, experiments and numerical simulations. Researchers exploited excitable media in two basic directions: forward problems and inverse problems. The forward problem is given a transition rule characterise the global behaviour of the system, which is from microscopic model to macroscopic phenomena. The forward research also includes the theoretical analysis and numerical simulation of excitable media. The inverse problem is given a description of some behaviour find a rule which replicates these behaviours. This is a process from macroscopic phenomena to microscopic model. As one of the most important tools to investigate the inverse problems, identification of a model directly from observed patterns is crucial for the study of excitable media. Coca and Billings [2001] identified a spatiotemporal system directly from data using a coupled map lattice model. Pan and Billings [2008] identified the Turing patterns using a similar model. Zhao and Billings et al. [2007] identified a practical pattern acquired from a real Belousov-Zhabotinsky reaction using a type of cellular automata model, the Greenberg-Hasting

model (GHM). Wei and Billings et al. [2009] identified a practical BZ pattern using a lattice dynamical wavelet neural network (LDWNN) model.

A new scalar coupled map lattice model (sCML) was recently proposed [Guo et al., 2010] which has the merits of both coupled map lattice and cellular automata. In the present paper the simple sCML model will continue to be studied. Section 2 introduces the general form of a sCML model and two examples identified from spatio-temporal patterns are given. The analysis of the sCML models is studied in Section 3 to illustrate how sCML models generate different patterns. Section 4 shows how to construct a sCML model based on several simple rules. Illustrative examples are given in Section 5 to demonstrate the application of the new results. Conclusions are finally given in Section 6.

2. General Form of the Scalar Coupled Map Lattice (sCML) Model

A lattice dynamical system (LDS) is a spatially extended dynamical system composed of a finite or infinite number of interacting dynamical systems, each assigned to a node, named as a cell, of a one- or multi-dimensional lattice of integers representing a discretisation of the physical space. The dynamics of a LDS can be viewed as a combination of local dynamics, involving the local state-space variables assigned to every cell, and spatial interactions [Billings & Coca, 2002].

An autonomous lattice dynamical system can be represented using a general CML model as

$$\mathbf{y}_1(\mathbf{k}) = \mathbf{f}(\mathbf{p}^{\mathbf{n}_k} \mathbf{q}^{\mathbf{n}_k} \mathbf{y}_1(\mathbf{k})) \quad (1)$$

Where $\mathbf{y}_1(\mathbf{k})$ represents the state-space variables assigned to the cell with a spatial coordinate $\mathbf{l} \in \mathbf{Z}^m$ of an m -dimensional lattice; $\mathbf{p}^{\mathbf{n}_k}$ is a temporal shift operator and $\mathbf{q}^{\mathbf{n}_k}$ is a multi-valued spatial shift operator.

As a simplification of the general CML model, the lattice equations can be assumed to be evolving on a uniform lattice, that is, the CML model is spatially invariant over the entire lattice. Define

$\mathbf{y}(\mathbf{k}) \triangleq \mathbf{y}_1(\mathbf{k})$ by dropping the spatial index \mathbf{l} and a LDS can be investigated by studying the dynamics of one specified cell.

In general, each cell can be coupled with all the other cells in the lattice. This represents a globally coupled LDS. Very often, however, the spatial interactions are restricted to only a finite set of neighbouring cells. In a reaction-diffusion model, these interaction effects are represented by the diffusion terms denoted as $\nabla^2 \mathbf{y}(\mathbf{k})$, where ∇^2 is the Laplace operator defined as

$\nabla^2 \mathbf{y}(\mathbf{x}, t) \triangleq \sum_{i=1}^m \frac{\partial^2 \mathbf{y}}{\partial x_i^2}$. The Laplace operator in two dimensions can be approximated using a finite

difference method as

$$\nabla^2 y_{l_1, l_2}^{(k)} \approx \frac{y_{l_1-1, l_2}^{(k-1)} + y_{l_1+1, l_2}^{(k-1)} + y_{l_1, l_2-1}^{(k-1)} + y_{l_1, l_2+1}^{(k-1)} - y_{l_1, l_2}^{(k-1)}}{(dl)^2} \quad (2)$$

It is natural to consider a measurement system for the excitable media system. The measurement variable may be a nonlinear function of the state-space variables, that is, $z(\mathbf{k}) = \mathbf{h}(\mathbf{y}(\mathbf{k}))$. A scalar coupled map lattice model can then be defined as

$$z(\mathbf{k}) = \mathbf{f} \left(p^m z, p^{m_i} (\nabla^2 z) \right) \quad (3)$$

where, z represents the only component measured from practical patterns; p is a temporal shift operator; ∇^2 is the Laplace operator, which represents the diffusion of component z ; \mathbf{f} is a nonlinear function of z at previous times, and the diffusion of z at previous times.

Two sCML models have been separately identified from a simulated spatio-temporal pattern and from a real Belousov-Zhabotinsky pattern [Guo et al., 2010]. These two models, the simulated pattern model and the real pattern model, are given as (4) and (5) below.

$$\begin{aligned} z(\mathbf{k}) = & 1.7981z(\mathbf{k}-1) + 1.88849z^2(\mathbf{k}-1) - 1.70921z^3(\mathbf{k}-1) \\ & - 0.820409z(\mathbf{k}-2) - 1.83072z^2(\mathbf{k}-2) + 1.65721z^3(\mathbf{k}-2) \\ & + 0.459467\nabla^2 z(\mathbf{k}-1) - 0.42561\nabla^2 z(\mathbf{k}-2) \end{aligned} \quad (4)$$

$$\begin{aligned}
z(k) = & 0.95013z(k-1) - 0.0424791z(k-2) + 1.86899 \times 10^{-5} z^4(k-1) \\
& - 5.73529 \times 10^{-5} z^3(k-1)z(k-2) + 6.28918 \times 10^{-5} z^2(k-1)z^2(k-2) \\
& - 0.00310803z^3(k-1) + 0.118357z^2(k-1) - 0.185982z(k-1)z(k-2) \\
& + 0.00779509z^2(k-1)z(k-2) + 3.0084 \times 10^{-6} z^4(k-2) \\
& - 2.71051 \times 10^{-5} z(k-1)z^3(k-2) - 0.0068082z(k-1)z^2(k-2) \\
& + 0.00207884z^3(k-2) + 0.0712825z^2(k-2) \\
& + 0.743265\nabla^2 z(k-1) - 0.354318\nabla^2 z(k-2)
\end{aligned} \tag{5}$$

The local dynamics of model (4) and model (5) are illustrated in Fig 1 (a) and (b). Fig 1 shows the excitability of both models, that is, a cell in a resting state is stable for a small perturbation (shown by the blue curves) while a perturbation with strength greater than a certain threshold can cause this cell to undergo a large excursion (shown by the red curves).

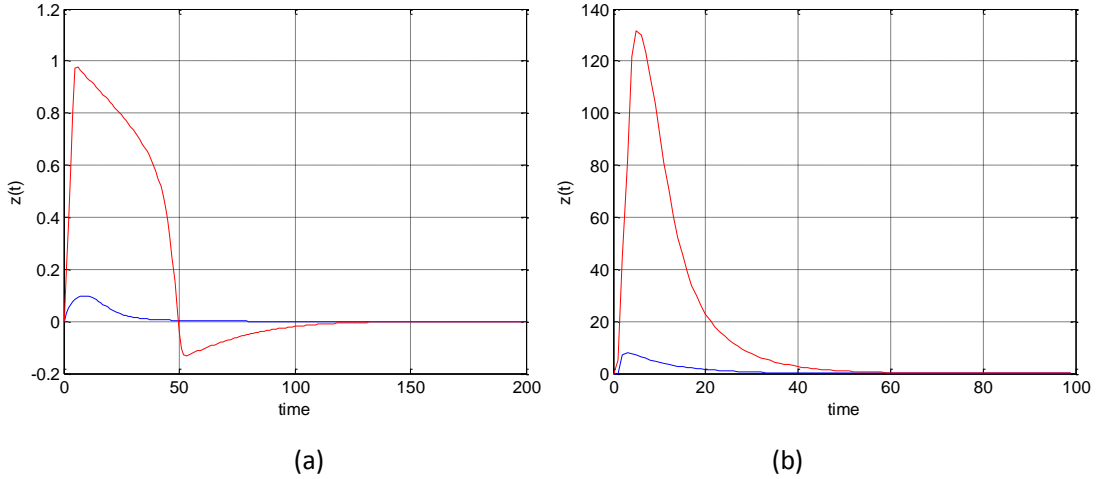


Fig 1 Local dynamics of the sCML models

(a) local dyanmics of model (4) (b) local dynamics of model (5)

Blue curves represent excitability for a small perturbation and red curves for a large perturbation

3. Analysis of the sCML model

3.1 Decomposition of the sCML model

Assume the general sCML model (3) is of a reaction-diffusion structure, that is, the delayed states

$p^m z$ and time-delayed diffusion terms $p^{m_u} (\nabla^2 z)$ affect the evolution of the state separately.

Therefore sCML model (3) can be rewritten of the form

$$z(k) = R(p^{m_t} z) + D(p^{m_u} (\nabla^2 z)) \quad (6)$$

Where function $R(p^{m_t} z)$ represents the reaction part and function $D(p^{m_u} (\nabla^2 z))$ represents the diffusion part of the sCML models. Obviously, both model (4) and (5) are of the reaction-diffusion form given in (6).

Define a *G-function* of the sCML model (6) as

$$g(p^{m_t} z) = R(p^{m_t} z) - z(k-1) \quad (7)$$

Then model (6) can be rewritten as

$$z(k) - z(k-1) = g(p^{m_t} z) + D(p^{m_u} (\nabla^2 z)) \quad (8)$$

The left hand side of equation (8) represents the change of component $z(k)$ over the sampling time; $g(p^{m_t} z)$ is the G-function which represents the contribution of the local dynamics to the evolution of excitable media. Term $D(p^{m_u} (\nabla^2 z))$ represents the contribution of the diffusion part.

Define *F-functions* of model (6) as the partial derivatives of the G-function $g(p^{m_t} z)$ with respect to $z(k-i)$ $i=1,2,\dots,m_t$, that is

$$f_i(p^{m_t} z) = \frac{\partial g}{\partial z(k-i)} \quad (9)$$

The F-functions describe how the previous states $z(k-i)$ affect the evolution of an excitable media.

Rewriting model (4) in the form of (8), the G-function is given as

$$g(p^{m_t} z) = 0.7981z(k-1) - 0.820409z(k-2) + 1.65721z^3(k-2) - 1.83072z^2(k-2) + 1.88849z^2(k-1) - 1.70921z^3(k-1) \quad (10)$$

Calculating the F-functions of model (4) with respect to $z(k-1)$ and $z(k-2)$ according to

formula (9) yields

$$\begin{aligned} f_1(g(p^m z)) &= 0.7981 + 2 \times 1.88849z(k-1) - 3 \times 1.70921z^2(k-1) \\ f_2(g(p^m z)) &= -0.820409 - 2 \times 1.83072z(k-2) + 3 \times 1.65721z^2(k-2) \end{aligned} \quad (11)$$

F-functions of model (4) are illustrated in Fig 2. In this example, f_1 and f_2 reduce to functions of only one variable in model (4) that is $f_1(p^m z) = f_1(z(k-1))$ and $f_2(p^m z) = f_2(z(k-2))$. Observe that F-functions f_1 and f_2 are similar in shape but take opposite signs.

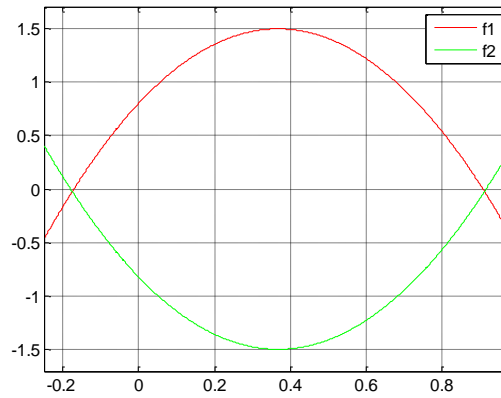


Fig 2 F-functions of model (4)

Consider sCML model (5) which was identified directly from real Belousov-Zhabotinsky reaction data. Repeating the same calculation, the G-function and F-functions of model (5) are given as (12) and (13) separately.

$$\begin{aligned} g(p^m z) &= -0.0499z(k-1) - 0.0424791z(k-2) + 1.86899 \times 10^{-5} z^4(k-1) \\ &\quad - 5.73529 \times 10^{-5} z^3(k-1)z(k-2) + 6.28918 \times 10^{-5} z^2(k-1)z^2(k-2) \\ &\quad - 0.00310803z^3(k-1) + 0.118357z^2(k-1) - 0.185982z(k-1)z(k-2) \\ &\quad + 0.00779509z^2(k-1)z(k-2) + 3.0084 \times 10^{-6} z^4(k-2) \\ &\quad - 2.71051 \times 10^{-5} z(k-1)z^3(k-2) - 0.0068082z(k-1)z^2(k-2) \\ &\quad + 0.00207884z^3(k-2) + 0.0712825z^2(k-2) \end{aligned} \quad (12)$$

$$\begin{aligned}
f_1(p^m z) &= -0.0499 + 4 \times 1.86899 \times 10^{-5} z^3(k-1) \\
&\quad - 3 \times 5.73529 \times 10^{-5} z^2(k-1)z(k-2) \\
&\quad + 2 \times 6.28918 \times 10^{-5} z(k-1)z^2(k-2) - 3 \times 0.00310803 z^2(k-1) \\
&\quad + 2 \times 0.118357 z(k-1) - 0.185982 z(k-2) + 2 \times 0.00779509 z(k-1)z(k-2) \\
&\quad - 2.71051 \times 10^{-5} z^3(k-2) - 0.0068082 z^2(k-2) \\
f_2(p^m z) &= -0.0424791 - 5.73529 \times 10^{-5} z^3(k-1) \\
&\quad + 2 \times 6.28918 \times 10^{-5} z^2(k-1)z(k-2) - 0.185982 z(k-1) \\
&\quad + 0.00779509 z^2(k-1) + 4 \times 3.0084 \times 10^{-6} z^3(k-2) \\
&\quad - 3 \times 2.71051 \times 10^{-5} z(k-1)z^2(k-2) - 2 \times 0.0068082 z(k-1)z(k-2) \\
&\quad + 3 \times 0.00207884 z^2(k-2) + 2 \times 0.0712825 z(k-2)
\end{aligned} \tag{13}$$

Fig 3 shows the F-functions of model (5). It is easy to see that F-functions f_1 and f_2 are again of the similar shape and take opposite signs.

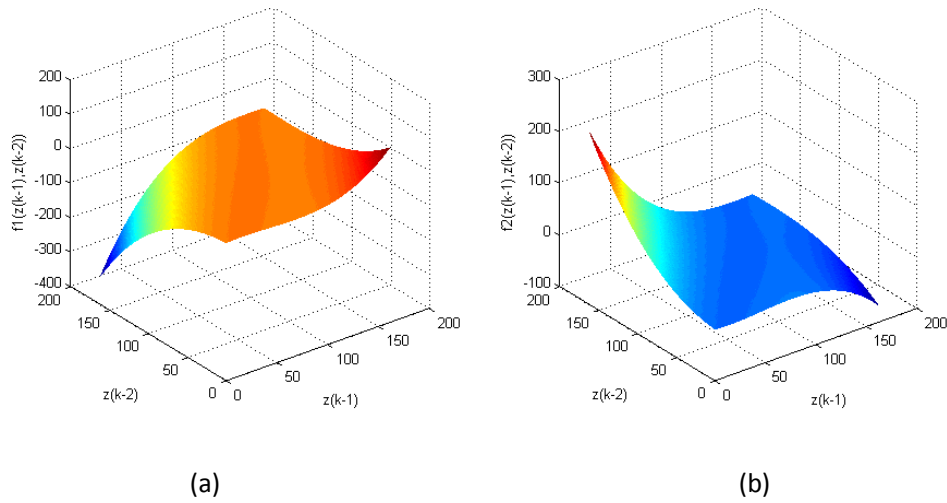


Fig3 F-functions of model (5)

$$(a) f_1(z(k-1), z(k-2)) \quad (b) f_2(z(k-1), z(k-2))$$

If $z(k-1)$ and $z(k-2)$ always take close values, $f_1(z(k-1), z(k-2))$ and $f_2(z(k-1), z(k-2))$ will only take values near the cross-sections along $z(k-1) = z(k-2)$, namely, $f_1(p^m z(k)) \Big|_{z(k-1)=z(k-2)}$ and $f_2(p^m z(k)) \Big|_{z(k-1)=z(k-2)}$.

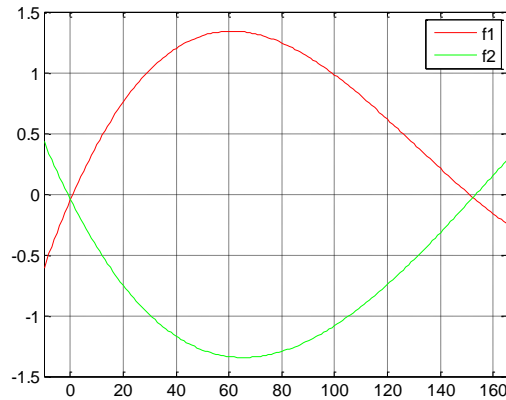


Fig4 Cross-sections of F-functions along $z(k-1)=z(k-2)$

The cross-sections of f_1 and f_2 in (13) along $z(k-1) = z(k-2)$ are shown in Fig 4. Comparing the curves in Fig 2 and Fig 4, it is easy to observe that the F-functions (or cross-sections of F-functions) of both model (4) and model (5) are of similar shapes although these two models were identified from two totally different systems.

3.2 Analysis of Excitability

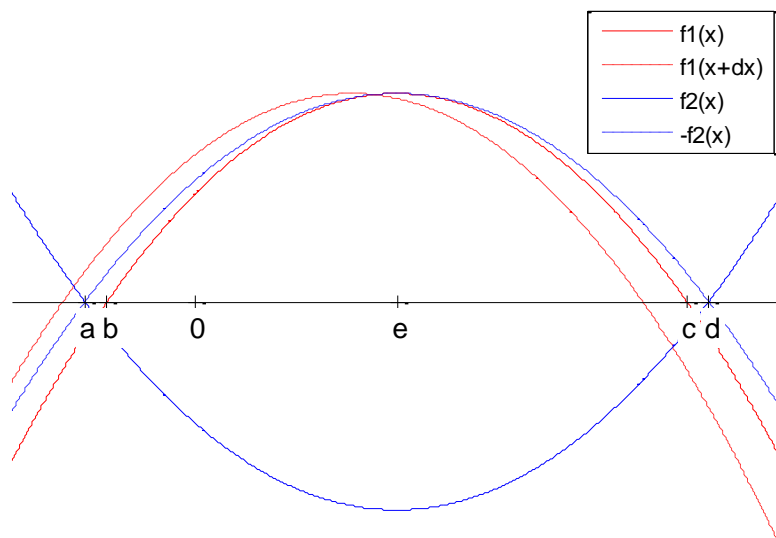


Fig 5 analysis of sCML models

Enlarging the F-functions in Fig 2 (and Fig 4) to produce Fig 5 where a and d are the points of intersection for f_1 and the real axis; b and c are the points of intersection for f_2 and the real axis satisfying $a < b < c < d$. Here, e is the point at which f_1 and f_2 reach the maximum and minimum almost simultaneously, and which divides the curves into left and right parts. Based on Fig 5, the sCML model will be analysed in two different aspects: the excitability and the

contribution of variables.

The shapes of f_1 and f_2 guarantee the excitable behaviour of the spatio-temporal system. Observe that $|f_1(0)| < |f_2(0)|$, which makes the zero point locally stable against a small disturbance. This coincides with the excitability property. However when the perturbation is large enough, the system will leave the equilibrium point and undergoes a long excursion to return to the equilibrium point. Assuming $z(k-1) = z(k-2) + dx$, when dx is large enough, $f_1(z(k-1)) > -f_2(z(k-2))$ in the region $[b, e]$ while $f_1(z(k-1)) < -f_2(z(k-2))$ in the region $[e, c]$. This means $z(k)$ will increase and then decrease back to the equilibrium state and this is a relatively longer journey compared with the case when the process is disturbed by a small disturbance.

3.3 Analysis of the Contribution of Variables

In Fig 2 (and Fig 4), the two intersections of function $f_1(z(k-1))$ and the real axis determine a special interval which is shown as $[b, c]$ in Fig 5. In this interval $f_1(z(k-1))$ always takes a positive value while $f_2(z(k-2))$ takes a negative value. According to the definition of the F-function in (9), this means that $z(k)$ increases with $z(k-1)$ increasing but decreases with $z(k-2)$ increasing. In other words, $z(k-1)$ plays the role of an activator and $z(k-2)$ plays the role of an inhibitor in the interval $[b, c]$. Hence the system is of an activator-inhibitor structure in $[b, c]$.

Since the responses of an excitable media system are independent on the strength of the perturbation only if the perturbation exceeds a certain threshold the system responses in Fig 1 roughly show the range of the state space \mathbf{S} in which $z(k)$ takes values. Comparing Fig 2 (and Fig 4) with Fig 1, it is easy to see that the interval between the intersections of f_1 and the

real axis is close to the state space \mathbf{S} . That is, roughly speaking, $z(k-1)$ acts as an activator and $z(k-2)$ acts as an inhibitor in \mathbf{S} .

4. Construction of sCML Models

The analysis results discussed in the preceding section will now be used to inform the construction of simple sCML models. Construction of a new sCML model is essentially an inverse routine of the analysis. The model will be constructed to possess the properties of excitable media. The F-functions $f_i(p^m z(k))$ defined in (9) of the shapes in Fig 5 should be constructed first of all. Obviously, different sCML models can be constructed by selecting different model structures and properly setting the corresponding coefficients. In this section only the simplest model will be considered. Several basic rules are proposed to construct a simple sCML model.

4.1 Construction of F-functions $f_i(p^m z(k))$

For simplicity, assume $f_1(p^m z(k))$ and $f_2(p^m z(k))$ are of the simplest form $f_1(p^m z(k)) \triangleq f_1(z(k-1))$ and $f_2(p^m z(k)) \triangleq f_2(z(k-2))$, that is f_1 is a function of $z(k-1)$ and f_2 a function of $z(k-2)$. In order to make the F-functions of the shape in Fig 5, the simplest structure that can be taken are second order polynomials. Denote the intersections between the derivative curves and the real axis as a, b, c , and d , where $a < b < c < d$. F-functions f_1 and f_2 can then be constructed as

$$f_1(z(k-1)) = -A_a (z(k-1) - b)(z(k-1) - c) \quad (14)$$

$$f_2(z(k-2)) = A_b (z(k-2) - a)(z(k-2) - d) \quad (15)$$

Where A_a and A_b determine the amplitude of the functions.

A_a and A_b should be chosen to make f_1 and $-f_2$ close enough. Moreover, A_a and A_b cannot be large numbers because the amplitudes of functions f_1 and f_2 are related to the

change rate of $z(k)$ in a sample interval otherwise the final model will be numerically unstable. The parameter a should be set to be very close to b , and c should be set close to d . This is because the difference between a and b is related to the excitation threshold. The threshold should be a very small value so that the resting cells can be excited owing to the diffusion effect. The state set \mathbf{S} where $z(k) \in \mathbf{S}$ can be determined by appropriately setting the distance between b and c .

4.2 Construction of G-function $g(p^m z)$

Model (4) and model (5) indicate that an excitable media can be described by a model with only one component and only first and second order time-delays of the components are needed. In this section the assumption that the evolution of a cell is only affected by $z(k-1)$, $z(k-2)$, and the associated diffusions will continue to be used to construction a simple sCML model. Based on this assumption, a total derivative of the G-function can be constructed

$$dg = f_1(z(k-1), z(k-2))dz(k-1) + f_2(z(k-1), z(k-2))dz(k-2) \quad (16)$$

The G-function can then be calculated by Integrating both side of equation (16).

$$\begin{aligned} &g(z(k-1), z(k-2)) \\ &= \int f_1(z(k-1), z(k-2))dz(k-1) + \int f_2(z(k-1), z(k-2))dz(k-2) + C \end{aligned} \quad (17)$$

The constant of integration C can be taken as zero to make $(0, 0)$ a fixed point of the system. For excitable media the zero fixed point should be locally stable so that the system will return to the equilibrium state after a small disturbance occurs.

4.3 Selection of the Diffusion Coefficients and the Final Model

To properly select the diffusion coefficients, two principles should be considered. Firstly, the diffusion should be large enough to excite the resting cells. Secondly, when an inhibitor diffuses faster than an activator, the equilibrium point may lose the stability because of the Turing bifurcation [Gierer & Meinhard, 1972; Turing, 1952] and then the system cannot be an excitable media system any more. Therefore the inhibitor is assumed to have a smaller diffusion rate as compared with activator so that spiral patterns can be generated. That is, the diffusion coefficient

d_1 of $z(k-1)$ takes a larger value than the diffusion coefficient d_2 of $z(k-2)$.

Until now all parts which a sCML model need have been constructed. Collecting all the results together gives the final sCML model takes the form

$$\begin{aligned} z(k) = & z(k-1) + \int -A_2 (z(k-1) - a)(z(k-1) - d) dz(k-1) \\ & + \int A_1 (z(k-2) - b)(z(k-2) - c) dz(k-2) \\ & + d_1 \nabla^2 z(k-1) - d_2 \nabla^2 z(k-2) \end{aligned} \quad (18)$$

where $a < b < c < d$ and $d_1 > d_2$.

Equation (18) is the simplest sCML model where the F-functions are a second order polynomial of only one variable. Of course more complex sCML models, for example a model like (5), can be constructed to satisfy some specific requirements by appropriately choosing the F-functions. However, even the simplest sCML model can generate complex patterns such as spiral waves and expanding target patterns. This will be illustrated in the next section.

5. Illustrative Examples

In this section, illustrative examples will be constructed following the rules developed in the last section. The excitability and bifurcations of this model will then be analysed. The simulations show that this simple model can generate complex spatio-temporal patterns.

5.1 Construction of a sCML Model

Following the procedure in Section 4, a sCML model is constructed as follows.

$$\begin{aligned} z(k) = & 1.7557z(k-1) + 0.1979z^2(k-1) - 0.024z^3(k-1) \\ & - 0.7633z(k-2) - 0.1952z^2(k-2) + 0.0237z^3(k-2) \\ & + 0.2\nabla^2 z(k-1) - 0.1\nabla^2 z(k-2) \end{aligned} \quad (19)$$

by setting the parameters in (14) and (15) as

$$a = -1.53, b = -1.5, c = 7, d = 7.03, A_2 = 0.072, A_1 = 0.071 \quad (20)$$

and the diffusion coefficients as

$$d_1 = 0.2, d_2 = -0.1 \quad (21)$$

In a spatially homogeneous condition where the diffusion effect is absent, the behaviours of the system will be dominated by the local dynamics of the system. Dropping the diffusion part of the model initially and simulating the model under perturbations of different strengths. The local dynamics of model (19) is illustrated in Fig 6 which shows the dynamical system damps off a small-strength perturbation but undergoes a long term response for the stronger perturbation. Fig 6 (b) shows the phase portrait of the dynamical system. Observe that in the phase portrait $(z(k-1), z(k))$ starting from pint (0, 0.4) leaves the symmetry line $z(k) = z(k-1)$ (the black line) first and then returns back to the symmetry line. From Fig 5, $|f_1(z(k-1)) - f_2(z(k-2))|$ increases with the difference $|z(k-1) - z(k-2)|$ increasing in region $[b, c]$. This means a perturbed cell is excited quickly from the resting state and then refracts slowly from the excited state.

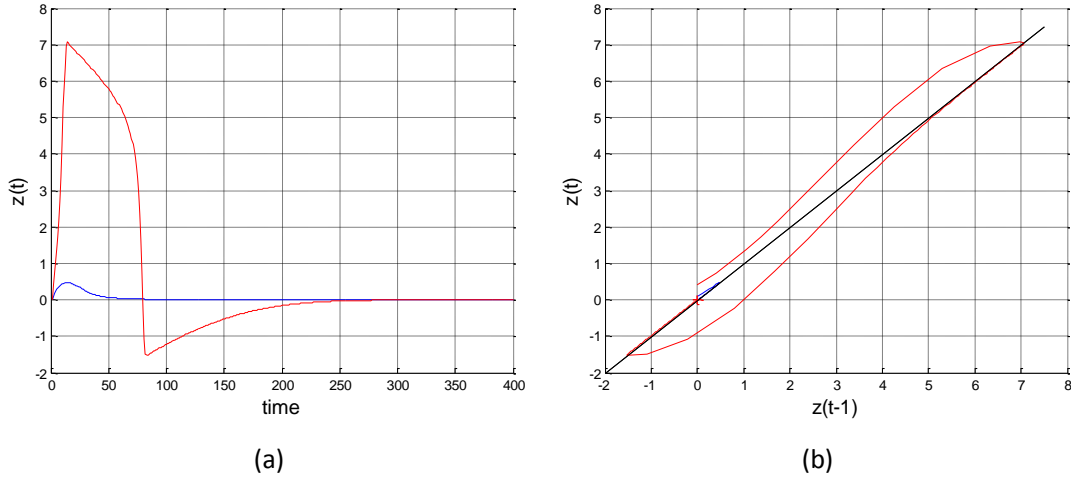


Fig 6 local dynamics of system (19)

(a) responses to different perturbations (b) phase portrait

5.2 Local Stability of the Resting State

Define $z_1(k) = z(k-1)$, $z_2(k) = z(k)$ and $\mathbf{z} = [z_1 \quad z_2]^T$. The local dynamics of model (19) can then be rewrite as the state-space equations.

$$\begin{cases} z_1(k) = g_1(z_1(k-1), z_2(k-1)) \\ z_2(k) = g_2(z_1(k-1), z_2(k-1)) \end{cases} \quad (22)$$

Where

$$\begin{cases} g_1(z_1(k-1), z_2(k-1)) = z_2(k-1) \\ g_2(z_1(k-1), z_2(k-1)) = 1.7557z_2(k-1) + 0.1979z_2^2(k-1) - 0.024z_2^3(k-1) \\ \quad - 0.7633z_1(k-1) - 0.1952z_1^2(k-1) + 0.0237z_1^3(k-1) \end{cases} \quad (23)$$

The fixed points of dynamical system can be calculated by solving the equation

$$\mathbf{z}(k) = \mathbf{g}(\mathbf{z}(k)) \quad (24)$$

Here, $\mathbf{z} = [0 \ 0]^T$ is the only root of equation (24), which corresponds to the resting state of an excitable media. The local stability of the fixed point can be analysed by considering the characteristic values of the following Jacobian matrix at the fixed point.

$$\mathbf{J} = \begin{bmatrix} \frac{\partial g_1}{\partial z_1} & \frac{\partial g_1}{\partial z_2} \\ \frac{\partial g_2}{\partial z_1} & \frac{\partial g_2}{\partial z_2} \end{bmatrix} \quad (25)$$

Substituting (23) into (25) yields

$$\mathbf{J} = \begin{bmatrix} 0 & 1 \\ -0.7633 & 1.7557 \end{bmatrix} \quad (26)$$

The characteristic equation of J can be written as

$$\lambda^2 - \text{tr}(J)\lambda + \det(J) = 0 \quad (27)$$

where $\text{tr}(J) = 1.7557$ is the trajectory of J and $\det(J) = -0.7633$ is the determinant of J .

Solving (27) yields $\lambda_1 = 0.9634$ and $\lambda_2 = 0.7923$. The resting state $(0, 0)$ is locally stable

because $|\lambda_{1,2}| < 1$.

5.3 Bifurcation Analysis of the Constructed sCML Model

A dynamical system loses stability at a fixed point as a pair of complex conjugate eigenvalues of the linearization around the fixed point cross the unit circle in the Z-plane. When this occurs, a limit cycle arises from the fixed point and a Hopf bifurcation happens. The sCML model may

undergo similar bifurcations when the parameters are slightly perturbed. From Fig 5 maintaining the relationship $a < b < c < d$, if the distance between b and c is shortened, the fixed point at $(0, 0)$ may lose stability and a limit cycle may be born.

Shortening the distance between point b and c by setting $a = -1.53, b = -1.5, c = 4, d = 4.03$. The maximums of the amplitude of F-functions will be less than half of the corresponding values in model (19). This means the evolution speed of the new system will significantly drop. Therefore reset $A_a = 0.1719, A_1 = 0.1682$ so that the new system can evolve at an appropriate rate. A new sCML model can then be given as

$$\begin{aligned} z(k) = & 2.0314z(k-1) + 0.2149z^2(k-1) - 0.0573z^3(k-1) \\ & - 1.0372z(k-2) - 0.2103z^2(k-2) + 0.0561z^3(k-2) \\ & + 0.2\nabla^2 z(k-1) - 0.1\nabla^2 z(k-2) \end{aligned} \quad (28)$$

Repeating the local stability analysis to give the Jacobian matrix

$$J = \begin{bmatrix} 0 & 1 \\ -1.0372 & 2.0314 \end{bmatrix} \quad (29)$$

The characteristic equation is

$$\lambda^2 - \text{tr}(J)\lambda + \det(J) = 0 \quad (30)$$

where $\text{tr}(J) = 2.0314, \det(J) = 1.0372$.

Solving (30) yields $\lambda_{1,2} = 1.0107 \pm 0.1252i$. But now the fixed point $(0, 0)$ is locally unstable because $|\lambda_{1,2}| > 1$. This means the excitable media system loses stability at point $(0, 0)$ when the parameters are adjusted from model (19) to model (28). Simulating the local dynamics of model (28), the system response to a perturbation and the phase portrait are illustrated in Fig 7 (a) and (b). Observe that state $(z(k-1), z(k))$ leaves initial point $(0, 0.4)$ and finally approaches a stable limit cycle which is of a different topology from the fixed point in model (19). This means a Hopf-like bifurcation occurs where a fixed point turns into a limit cycle as the parameters are adjusted.

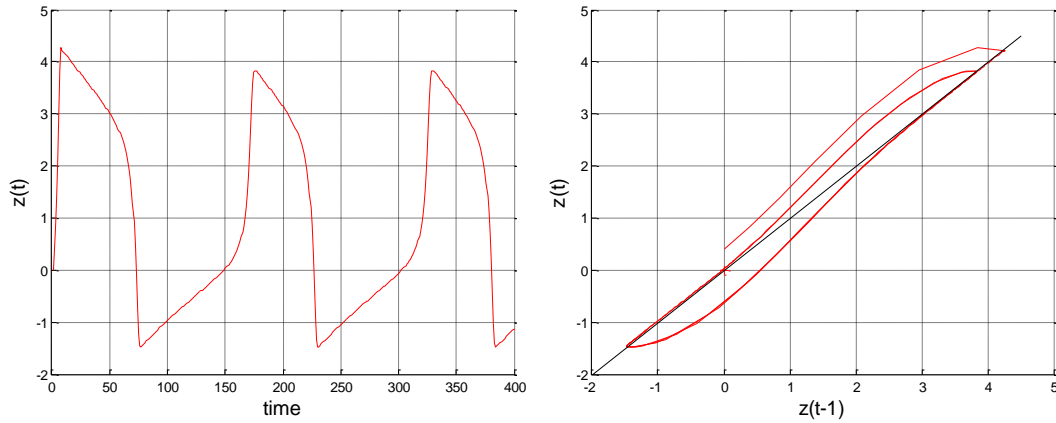


Fig 7 local dynamics of system (28)

(a) responses to an perturbation (b) phase portrait

A similar bifurcation happens when the values of c and d in model (19) are maintained but the values of a and b are reduced. The different regions in the parametric space b - c are shown in figure 8 where $a = b - 0.03$, $d = c + 0.03$. In region 2, a stable equilibrium at $(0, 0)$ exists. In region 3 a stable limit cycle exists. In region 1 and 4, the system is unstable at $(0, 0)$, that is the response of the system to an initial perturbation will not be convergent to any bounded set.

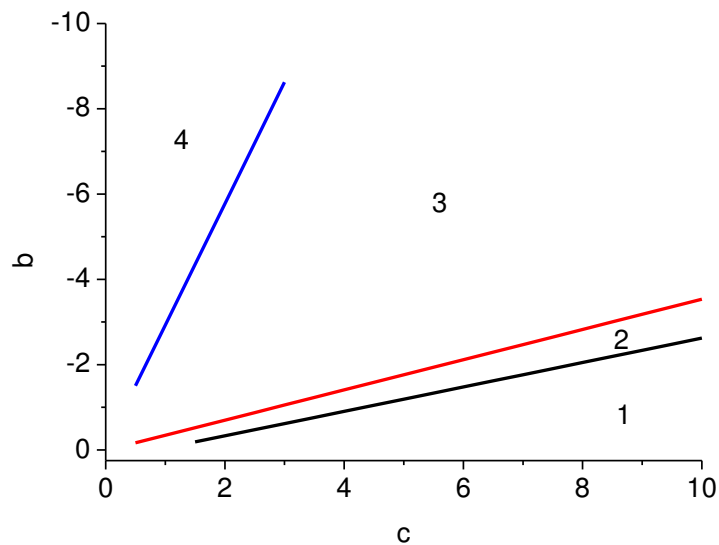


Fig 8 Parametric regions of the sCML model (19)

This bifurcation may not be a strict Hopf bifurcation because usually more than one parameter will change when the bifurcation happens. This kind of bifurcation is important for excitable media. Different patterns would be observed if the model is simulated before and after the

Hopf-like bifurcation. For example, spiral patterns will be generated before the Hopf-like bifurcation, while target-like patterns will be generated after the bifurcation. If $z(k)$ represents the concentration of a component in an excitable medium, the bifurcation will be coincident with the real dictyostelium discoideum experiment [Lee et al., 1996]. Lee and co-workers showed that using the density as a control parameter, spiral waves dominated the pattern when the density was high whereas circular waves were dominant in the pattern at low densities.

5.4 Simulation of the Designed sCML Models (19) and (28)

Combining the local dynamics with the diffusion effects, different patterns can be generated by simulating the sCML models. The sCML model (19) was simulated on a 256X256 square lattice with a periodic boundary condition where a von Neumann neighbourhood was selected to describe the diffusion of components. The simulation was started from a purely random initial state. A snap shots of the simulated pattern at $k=500$ is illustrated in Fig 9 (a) which shows a typical spiral pattern.

For different values of the parameters, the sCML model exhibits different spatio-temporal patterns. Resetting the parameters as model (28) and simulating the model on the same lattice, this time with a zero initial condition and a spot disturbance in the centre produces typical expanding target-like patterns. A snap shot of the simulated patterns at $t=500$ is shown in Fig 9 (b).

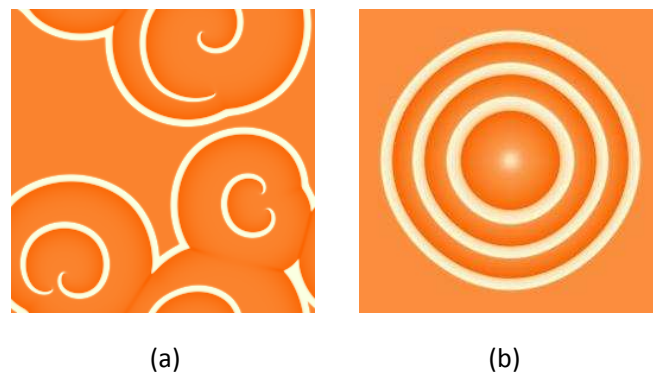


Fig 9 Simulation of sCML models

(a) the pattern generated by simulating model (19) (b) the pattern generated by simulating

6. Conclusions

Scalar coupled map lattice models are a new class of model for the description, identification and analysis of excitable media. Guo and co-workers [2010] showed the power of the new sCML model in identification. The current paper was presented as detailed analysis of the sCML model from different aspects to reveal the advantages of the new SML model in the interpretation of the excitable media.

The new sCML model possesses several significant advantages. This model can easily be identified from real data since only one component is needed. It has been shown that the model can easily be constructed based on several simple rules. The model can be used to analyse the behaviours of excitable media and to build a connection between the physical phenomena and the model parameters. It has been shown how new pattern formations can arise so that different spatio-temporal patterns can be generated by appropriately adjusting the parameters.

Acknowledgement

The authors gratefully acknowledge support from the UK Engineering and Physical Science Research Council (EPSRC) and the European Research Council (ERC).

References

- Barkley, D. [1991]. "A model for fast computer-simulation of waves in excitable media." *Physica D*, **49**, 61-70.
- Billings, S. A., &Coca, D. [2002]. "Identification of coupled map lattice models of deterministic distributed parameter systems." *International Journal of Systems Science*, **33**, 623-634.
- Chua, L. O. [2007]. *A Nonlinear Dynamics Perspective of Wolfram's New Kind of Science*, (World Scientific Publishing Co., Inc.).
- Chua, L. O., &Yang, L. [1988]. "Cellular neural networks: Theory." *IEEE transactions on circuits and systems*, **35**, 1257-1272.
- Coca, D., &Billings, S. A. [2001]. "Identification of coupled map lattice models of complex spatio-temporal patterns." *Physics Letters, Section A: General, Atomic and Solid State Physics*,

287, 65-73.

- Difrancesco, D., & Noble, D. [1985]. "A model of cardiac electrical activity incorporating ionic pumps and concentration changes." *Philosophical Transactions of the Royal Society of London Series B-Biological Sciences*, **307**, 353-398.
- Field, R. J., Noyes, R. M., & Koros, E. [1972]. "Oscillations in chemical systems 2. through analysis of temporal oscillation in bromate-cerium-malonic acid systems." *Journal of the American Chemical Society*, **94**, 8649-64.
- FitzHugh, R. [1955]. "Mathematical models of threshold phenomena in the nerve membrane." *Bulletin of Mathematical Biology*, **17**, 257-278.
- Fortuna, L., Arena, P., Bálya, D., & Zarándy, Á. [2001]. "Cellular Neural Networks: A Paradigm for Nonlinear Spatio-Temporal Processing." *IEEE Circuits and Systems Magazine*, **1**, 6-21.
- Gerhardt, M., Schuster, H., & Tyson, J. J. [1990]. "A cellular automaton model of excitable media including curvature and dispersion." *Science*, **247**, 1563-1566.
- Gierer, A., & Meinhard, H. [1972]. "Theory of biological pattern formation." *Kybernetik*, **12**, 30-39.
- Greenberg, J. M., & Hastings, S. P. [1978]. "Spatial patterns for discrete models of diffusion in excitable media." *Siam Journal on Applied Mathematics*, **34**, 515-523.
- Guo, Y., Zhao, Y., Billings, S. A., & Coca, D. [2010]. "Identification of excitable media using a scalar coupled map lattice model." *International Journal of Bifurcation and Chaos*, **20**, 2137-2150.
- Kawasaki, K., Suzuki, M., & Onuki, A. [1990]. "Formation, Dynamics, and Statistics of Patterns." World Scientific.
- Lee, K. J., Cox, E. C., & Goldstein, R. E. [1996]. "Competing Patterns of Signaling Activity in Dictyostelium Discoideum." *Physical Review Letters*, **76**, 1174-1177.
- Pan, Y., & Billings, S. A. [2008]. "The identification of complex spatiotemporal patterns using Coupled Map Lattice models." *International Journal of Bifurcation and Chaos*, **18**, 997-1013.
- Turing, A. M. [1952]. "The chemical basis of morphogenesis." *Philosophical Transactions of the Royal Society of London Series B-Biological Sciences*, **237**, 37-72.
- Wei, H. L., Billings, S. A., Zhao, Y. F., & Guo, L. Z. [2009]. "Lattice Dynamical Wavelet Neural Networks Implemented Using Particle Swarm Optimization for Spatio-Temporal System Identification." *IEEE Transactions on Neural Networks*, **20**, 181-185.
- Zhao, Y., Billings, S. A., & Routh, A. F. [2007]. "Identification of excitable media using cellular automata models." *International Journal of Bifurcation and Chaos*, **17**, 153-168.
- Zykov, V. S. [2008]. "Excitable media." *Scholarpedia*, **3**, 1834.